IOP PUBLISHING JOURNAL OF PHYSICS D: APPLIED PHYSICS

J. Phys. D: Appl. Phys. **41** (2008) 024005 (13pp) doi:10.1088/0022-3727/41/2/024005

Low angle forward reflected neutral beam source and its applications

B J Park[1], S W Kim[1], S K Kang[1], K S Min[1], S D Park[1], S J Kyung[1], H C Lee[1], J W Bae[1], J T Lim[1], D H Lee[3] and G Y Yeom[1,2]

[1] Department of Advanced Materials Engineering, SungKyunKwan University, Suwon, South Korea
[2] The National Program for Tera-level Nanodevices, Hawolgok-dong, Sungbuk-ku, Seoul, South Korea
[3] Samsung Electronics Co. Ltd., Memory Division, Yongin-city, Gyeonggi-do, South Korea

E-mail: gyyeom@skku.edu

Received 31 August 2007, in final form 16 October 2007
Published 4 January 2008
Online at stacks.iop.org/JPhysD/41/024005

Abstract

As one of the many nano-device fabrication techniques employed in the semiconductor industry, neutral beams are being examined using various methods to solve possible charge-related problems that occur during device processing. This review introduces a neutral beam generated by surface neutralization of an ion beam using a low angle forward reflection technique and explains its application to various areas such as surface treatments and etching. The neutralization efficiency of an ion beam using a low angle forward reflection technique was approximately 99.7%. When a metal-oxide-semiconductor device was etched using a reactive neutral beam, it was confirmed that charge-related problems such as aspect-ratio-dependent etching and gate oxide charging could be removed using reactive neutral beam etching instead of conventional reactive ion etching. Neutral beams can be beneficial to other devices such as the III-V device and field emission device.

(Some figures in this article are in colour only in the electronic version)

1. Introduction

Reactive ion etching (RIE) is one of the key technologies in the fabrication of deep submicrometre silicon-based integrated circuits. However, conventional RIE techniques can have serious disadvantages for future device fabrication due to charged particles and UV photons causing increased gate oxide breakdown, charging, etc. It is believed that these problems will become more serious as the critical dimensions of the device shrink to a few nanometres size [1–6]. Therefore, there is a need to develop novel semiconductor processing equipment and processing techniques that can cope with the issues caused by the integration of future semiconductor devices and the decrease in the design rule to the sub-nano scale. One of the methods being investigated by many researchers is etching using a reactive neutral beam [7].

The formation of a reactive neutral beam for the etching of semiconductor materials has been examined by many researchers and can be categorized into three methods: the use of gas dynamics (hyperthermal neutral beam), ion–neutral charge exchange collisions, and the surface recombination of ion–electrons (surface charge exchange collision) [8–25]. Gas dynamics obtain their neutral beams by injecting a reactive neutral particle through the heating of reactive gases using a laser beam to decompose the gas molecules and accelerate the decomposed gas molecules to have a kinetic energy of approximately 2–20 eV or by injecting a heated reactive neutral particle through the pressure differences under adiabatic conditions without a laser beam. Through these methods, a supersonic neutral beam for the etching of semiconductor materials can be obtained. However, it is difficult to scale these methods to larger areas for commercial device processing applications [8–14]. In the case of the ion–neutral charge exchange method, conventional plasmas, such as high density plasmas, are generated at low pressure and the reactive ions in the plasma are accelerated to the vacuum chamber using a grid system. This is followed by the formation of a neutral beam by the forward charge exchange collision of the ions with the neutral atoms in the vacuum chamber during the travel of ions in the chamber [15–20]. Although a large-size neutral beam can be made using this charge exchange method, it is difficult to form a parallel neutral beam and for the neutral beam to have a high neutral percentage due to the mixture of ions in the beam that were not forward scattered with the neutrals

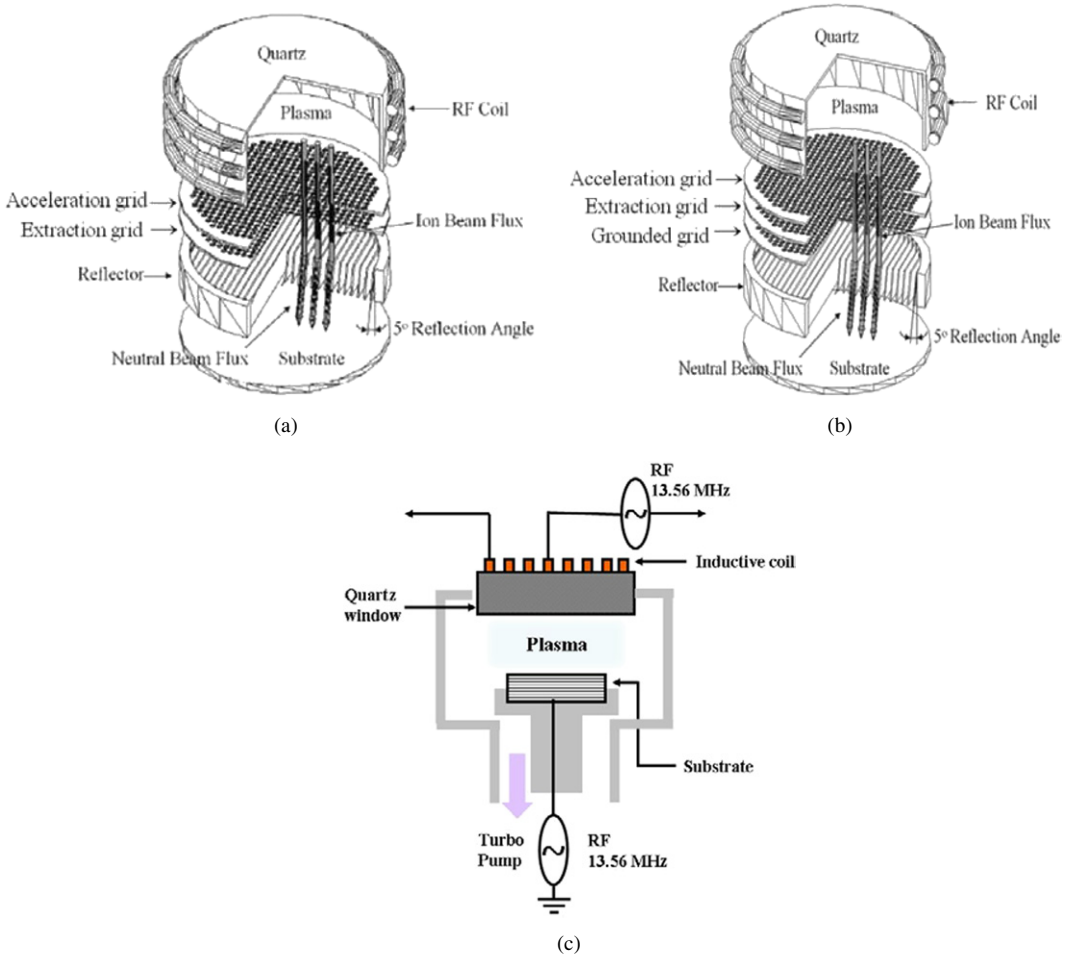

Figure 1. Schematic diagram of the low angle forward reflected neutral beam etching system used in the experiment. (*a*) two-grid system and (*b*) three-grid system. Schematic diagram of an ICP system used in the experiment to compare with the neutral beam system is also shown in (*c*). The figure is reprinted from [27].

while travelling through the vacuum chamber. An additional retarding-grid system, a magnetic field or a vertically aligned electric field is needed over the substrate to remove the ions in the beam. The most commonly examined methods for neutralizing ions employ the neutralization of the ions on a reflector surface [21–26]. The formation of a neutral beam through the reflection of a surface can be accomplished by reflecting the ions on a flat sidewall surface of grid holes located outside of the plasma source [22–24], or by reflecting the ion beam on a reflecting plate [21, 25, 26]. This method of neutralization not only provides high flux and a parallel neutral beam but can also form a uniform large-scale neutral beam for the processing of commercial silicon substrates.

Among the various methods for producing a reactive neutral beam using ion–electron surface neutralization, this review paper describes the formation of a reactive neutral beam by the low angle forward reflection of ions extracted from a two or three-grid ion gun on a flat reflector surface and reviews the application data obtained using this neutral beam technique. Most applications were related to the charge-induced damage to the semiconductor devices during the device processing using plasma processing. In particular, the possibilities of processing semiconductor devices without causing charge-related issues during top–down device processing were identified from the various applications using this neutral beam method.

2. Characteristics of low angle forward reflected neutral beam

2.1. Low angle forward reflected neutral beam apparatus

The reactive neutral beam source fabricated by the low angle forward reflection technique consisted of an inductively coupled plasma (ICP) ion gun with two or three grids and a planar reflector. Due to the separation of the neutral beam source into the ion gun and a reflector, where the ion gun accelerates and the planar reflector neutralizes the ion beam this neutral beam has advantages in that the neutral beam energy can be varied through the acceleration and deceleration of the ion beam using the grid system even though the flux of the neutral beam can be slightly lower than the neutral beam flux obtained by other surface neutralization techniques due to the grid system. Figure 1 shows a schematic diagram of the neutral beam source fabricated using the low angle forward reflection technique. The diameter of the ICP ion gun was 15 cm and the radio frequency (rf) power applied to the ion gun was varied from 100 W to 1 kW at a frequency of 13.56 MHz. The ions

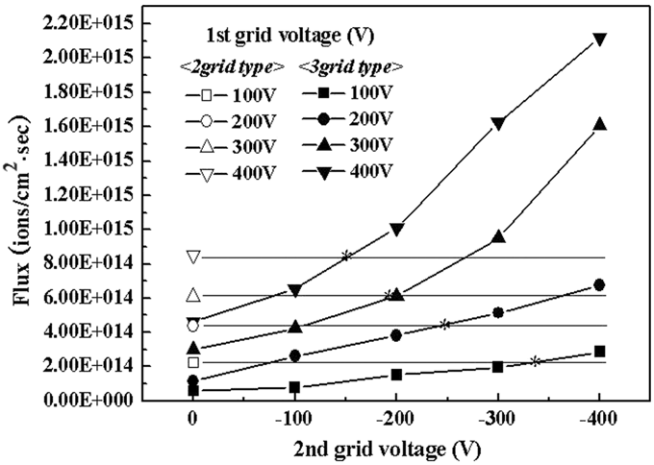

Figure 2. Ion flux measured as a function of 2nd grid voltage for the three-grid ion gun for various 1st grid voltages. Ion flux obtained as a function of various 1st grid voltages for the two-grid ion gun was also included as a comparison. The figure is reprinted from [27].

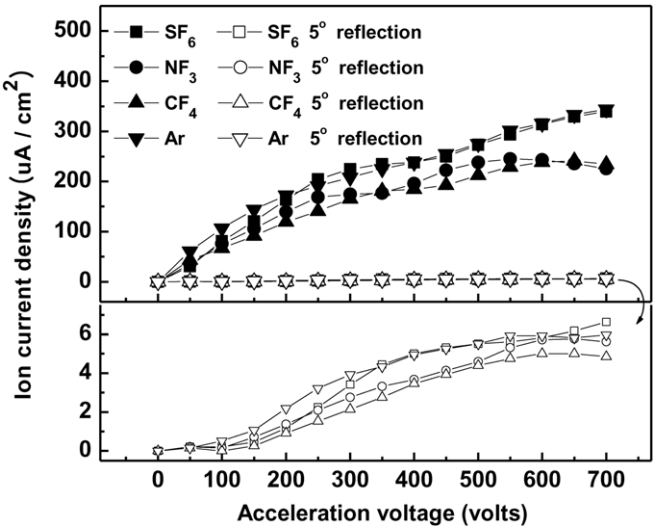

Figure 3. Ion current density as a function of the ion source acceleration voltage with/without reflector for various gases such as SF_6, NF_3, CF_4 and Ar (distance between the reflector and Faraday cup: 5 cm; gas flow rate: 7 sccm). The figure is reprinted from [28].

from the plasma in the gun were extracted using a two-grid or three-grid assembly with the opening percentage of the grid system of approximately 47%. In the two-grid system shown in figure 1(*a*), a potential ranging from +30 to +700 (V_a) was applied to the 1st grid located close to the plasma of the ion gun (acceleration grid). The 2nd grid located outside of the gun was grounded. In the three-grid system shown in figure 1(*b*), a potential ranging from +30 to +700 V (V_a) was applied to the 1st grid located close to the source (acceleration grid), a potential of 0 to −700 V (V_e) was applied to the 2nd grid (extraction grid) and the grid located outside the ground was grounded. Figure 2 gives a comparison of these grid systems. The result showed that the three-grid system showed a higher flux without changing the energy of the ion beam extracted compared with the two-grid system at the 2nd grid voltage higher than a certain potential. In addition, using the three-grid system, the flux of the ion beam could be varied without changing the energy of the beam while a change in the first grid potential changed both the flux and energy of the beam in a similar manner to the two-grid system. Therefore, recent studies on the neutral beam use a three-grid system instead of a two-grid system [27]. The currents flowing at the grids as a function of the voltage applied to the grids, which are beneficial for understanding the neutralization efficiency, could be measured using current meters mounted on the grids. The reflectors were made from a parallel stack of graphite supported by an aluminium block, with the axes of the reflector fabricated to make an angle of 5° to the ion beam direction. The plates of the reflector were matched to each hole of the grid of the ion source, and the depth of the reflector plate was optimized to reflect all the parallel ions extracted from the ion source and neutralize the extracted ions.

2.2. Measurement of neutralization percentage for various gases

The neutralization efficiency was estimated by measuring the ion flux (J_a) extracted from the ion source before reflecting on the reflector and the ion flux (J_b) extracted from the reflector after the reflection under the same process conditions using a Faraday cup, and the ratio of $(J_a - J_b) \times 100/J_a$ was taken as the neutralization efficiency.

Figure 3 shows the effect of the reflector (with and without a reflector in front of the ion source) and acceleration voltage on the ion current density measured using a Faraday cup for the gases SF_6, NF_3, CF_4 and Ar on the estimation of the neutralization efficiency of the two-grid system neutral beam source [28]. As shown in the figure, the measured ion current density increased with increasing acceleration grid voltage due to the increased extraction of ions at the higher voltage. There were no significant differences in the measured ion current density values between the different gases, even though Ar and SF_6 showed a slightly higher ion current density than CF_4 and NF_3. However, when measurements were carried out in the presence of the reflector, the ion current density was significantly lower than measured without the reflector for all the gases investigated. The significant decrease in ion current density detected with the reflector for all the gases appears to be related to the neutralization of ions during reflection at the reflector. The estimated neutralization efficiency of the reflector was approximately 99.7% under these experimental conditions.

3. Etch damage evaluation of the semiconductor devices etched by the low angle forward reflected neutral beam

Using the reactive neutral beam fabricated with the low angle forward reflection (three-grid type), semiconductor devices, such as metal-nitride-oxide-silicon (MNOS) and metal-oxide-semiconductor (MOS) devices, were etched, and the possible charge damage was estimated and compared with that using conventional ICP etching. The etch damage related to charging or UV damage was estimated using a capacitance–voltage

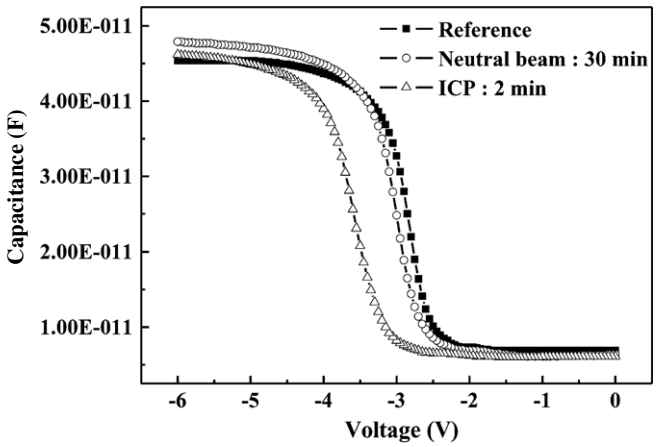

Figure 4. *C–V* characteristics of the NMOS device exposed to the oxygen neutral beam and inductively coupled plasma in 200 μm × 200 μm. The figure is reprinted from [29].

(C–V) technique and the breakdown voltage of the current–voltage (I–V) relation of the fabricated devices was determined using a CHARM®-2 wafer test. In addition, the RIE lag effect or aspect-ratio-dependent etching (ARDE), which originates from charging during the RIE, was also evaluated.

3.1. C–V, I–V characteristics of MOS/NMOS devices

The etch damage caused by the charged particles and UV photons during exposure to the low angle forward reflected oxygen neutral beam and oxygen ICP was compared using the C–V technique. Figures 4 and 5 show the I–V relationship and results, respectively [29]. For the C–V measurement, the NMOS device (200 × 200^2 μm^2 size NMOS composed of Al (500 nm)/Si_3N_4 (50 nm)/SiO_2 (2 nm) on the p-type Si was used, and MOS device (200 × 200^2 μm^2 size MOS composed of Al (500 nm)/SiO_2 (2 nm) on p-type Si) was used for the I–V measurement.

In figure 4, in order to compare ICP etching with neutral beam etching, the devices were exposed for a set time to remove a 1.5 μm thick photoresist, which corresponds to 2 min of ICP (rf power: 500 W, bias V: −100 V) and 30 min of the neutral beam etching (rf power: 500 W, acceleration voltage: 400 V, extraction voltage: −100 V). As shown in figure 4, in the case of the MNOS devices exposed to the ICP, the flat band voltage was shifted, while there was no noticeable shift in the flat band voltage observed in the MNOS devices exposed to the oxygen neutral beam. The shift in the flat band voltage is believed to originate from the creation of a positive charge at the SiO_2/Si interface during etching [30]. Therefore, the charging damage caused by etching appears to occur for conventional ICP etching while no such charging damage is observed for neutral beam etching.

Figure 5 shows the I–V characteristics of the MOS devices measured after exposure to the oxygen neutral beam from 0 (reference) to 60 min and to the oxygen ICP from 0 (reference) to 2 min to estimate the degree of radiation damage. The other conditions were the same as those shown in figure 4. As shown in the figure, in the case of the MOS devices exposed to the oxygen ICP, the increase in exposure time from 0 to 2 min

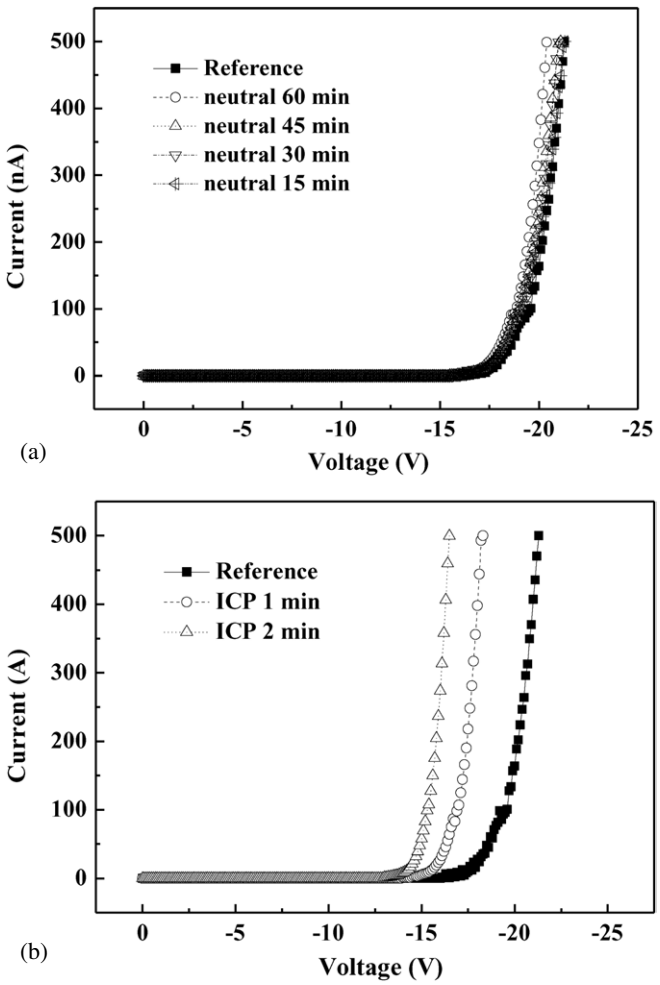

Figure 5. I–V characteristics of the MOS devices exposed to (*a*) oxygen neutral beam and (*b*) oxygen ICP as a function of the exposure time. The figure is reprinted from [29].

decreased the breakdown voltage of the MOS device. On the other hand, the MOS devices exposed to the oxygen neutral beam for up to 60 min did not show any significant change in the breakdown voltage. The decrease in the breakdown voltage observed with increasing exposure time to the ICP is believed to be related to local band bending of the energy band near the gate/SiO_2 interface due to the increase in the trap charge at the Si/SiO_2 interface. Therefore, tunnelling and avalanche breakdown occurred at a lower voltage. Because no charge trapping was observed during exposure to the neutral beam, charge-related problems such as a flat band voltage shift and a decrease in the breakdown voltage caused by etching using the charged particles, such as RIE, are believed to be decreased significantly by neutral beam etching.

3.2. Analysis of charging damage using CHARM®-2 monitoring wafers

In industry, the CHARM®-2 wafer technique, which is one of the commercially available charge estimation wafers, is widely used to estimate possible process induced damage. The CHARM®-2 wafer contains devices that are sensitive to positive charge, negative charge and UV photons. Therefore,

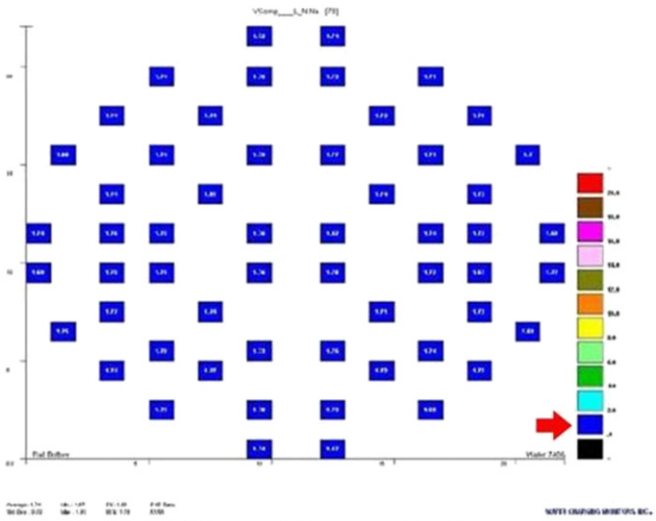

(a)

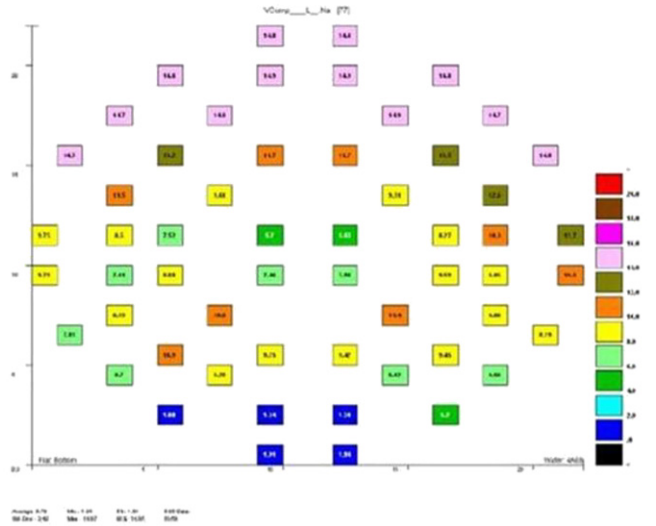

(b)

Figure 6. Charging map measured using CHARM® 2 monitoring wafers after etching by (*a*) oxygen neutral beam (5 min) and (*b*) oxygen ICP (30 s). The etch time was selected by considering the etch rate using similar etching conditions to those shown in figure 4.

the wafer can not only be used to measure the *I*–*V* characteristics of the charging source by the devices on the surface of the wafer but are also used to measure the process induced damage through the charging current measured by the *I*–*V* characteristics of the devices [31, 32]. The CHARM®-2 wafers were also exposed to the oxygen neutral beam etcher for 5 min, and to the ICP for 30 s by considering the etch rate using similar etching conditions shown in figure 4. Figure 6 shows the results for positive charging at various wafer locations, and table 1 shows the average values for positive charging, negative charging and UV damage in the wafer. As shown in figure 6, after exposure to the neutral beam for 5 min, there was no significant positive charging observed throughout the wafer surface while significant positive charging in addition to a change in charging damage on the wafer surface could be observed for exposure to the ICP for 30 s. In particular, as shown in table 1, not only positive charging but also negative

Table 1. Degree of charge damage and UV photon damage measured with CHARM®-2 monitoring wafers after the oxygen neutral beam treatment (60 s and 5 min) and ICP treatment (30 s).

Condition(s)	Neutral beam (60 s)	Neutral beam (5 min)	ICP (30 s)
UV (difference)	+0.11	+0.67	+3.92
Positive charge (difference)	+0.01	+0.00	+11.1
Negative charge (difference)	−0.00	−0.01	−6.5

charging and UV damage could be observed after exposure to the ICP for 30 s, while no significant change in positive charging, negative charging and UV damage was observed after exposure to the neutral beam etcher for both 60 s and 5 min.

3.3. Removal of ARDE effect

During the RIE of a material patterned with a photoresist with different opening widths, the ARDE effect, which shows a slower etch rate at a location with a narrower opening width can be observed as a result of a charging effect. During the etching, the top side of the pattern was charged negatively by randomly incident electrons while the bottom of the etched material was charged positively as a result of the vertically incident positive ions through the sheath voltage formed between the plasma and the substrate. Therefore, an electric field is formed between the photoresist and the etched material. Moreover, the trajectory of the incident positive ions during the RIE is bent due to the electric field, and as the aspect ratio of the pattern becomes higher and higher, it becomes increasingly difficult for the incident positive ions to reach the bottom of the etched material, which reduces the etch rate. Finally, etching stops due to the lack of positive ions reaching the bottom of the material [33–35]. Generally, this ARDE effect can be minimized or removed by controlling the mixture of etch gases, using a different gas mixture, and controlling the operating pressure. However, as the design rule of the device decreases to the sub-nano scale <50 nm, the ARDE effect will become more significant, and control of the ARDE effect by controlling the operating parameters during etching by RIE will become increasingly difficult.

Figure 7 showed the profiles of polysilicon on silicon substrates and SiO_2/silicon substrates etched by (*a*) an ICP, (*b*) an ion beam and (*c*) a neutral beam. For ICP etching, rf power of 700 W, a bias voltage of −75 V and 5 mTorr SF_6 were used to etch the polysilicon, while rf power of 400 W, an acceleration voltage of 400 V, an extraction voltage of −100 V and 0.3 mTorr SF_6 were used for neutral beam etching and ion beam etching. In order to operate as ion beam etching, the reflector installed in front of the ion gun of the neutral beam source was removed. As shown in figure 7, in the case of the ICP etching shown in figure 7(*a*), a wide opening area with a small aspect ratio was etched more than the narrow opening area with a high aspect ratio. The differences were larger for the polysilicon etching on SiO_2/silicon substrate.

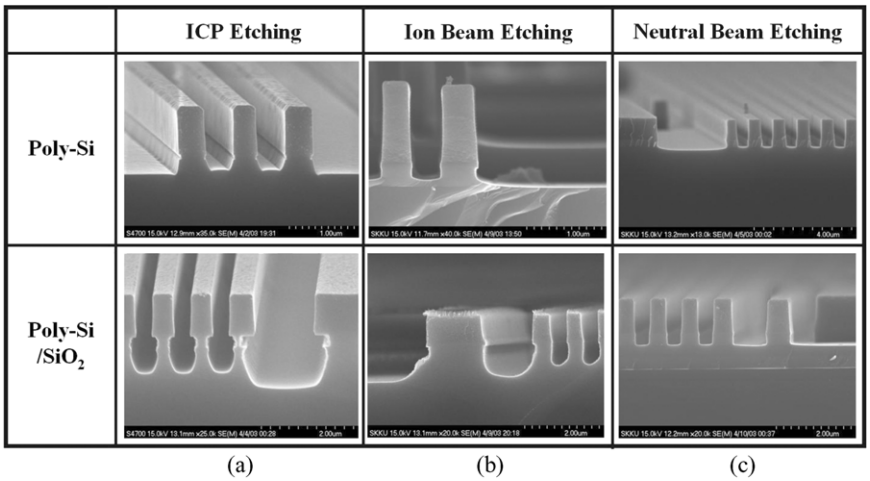

Figure 7. SEM etch profiles of the polysilicon features with different aspect ratios between the open area ($>1.5\ \mu$m) and the trench area (400 nm) covered by photoresist observed after etching by (*a*) an ICP, (*b*) a reactive ion beam and (*c*) a neutral beam with SF_6. As samples, polysilicon Si and polysilicon SiO_2/Si were used. The figure is reprinted from [36].

Therefore, a significant ARDE effect could be observed for ICP etching. However, the ARDE effect almost disappeared when the polysilicon was etched using the neutral beam, as shown in figure 7(*c*), possibly due to the lack of charging during etching. As mentioned above, the differences in etching conditions can cause differences in the ARDE effect. Therefore, the polysilicon was etched with an ion beam under the same etch conditions used for neutral beam etching just by removing the reflector attached to the neutral beam source. As shown in figure 7(*b*), a similar ARDE effect to ICP etching could be observed [36].

One of the practical cases related to the ARDE effect is the Si_3N_4 spacer etching of MOS device fabrication. Figure 8(*a*) shows the gate area after the deposition of a 50 nm thick Si_3N_4 layer uniformly and conformally around the polysilicon/WSi features. For device fabrication, the Si_3N_4 deposited on top of the feature and the Si_3N_4 on the trench area should be etched by the same amount until the Si_3N_4 on the trench area is removed completely [36]. Conventional RIE etches the Si_3N_4 on the bottom of the trenches slower than that on the top of the features due to the ARDE effect caused by charging. Therefore, excessive overetching on the top of these features is unavoidable. However, when a neutral beam is used, as shown in figure 8(*b*), both areas could be etched by nearly the same amount because the ARDE effect almost disappeared by the significant reduction of charging.

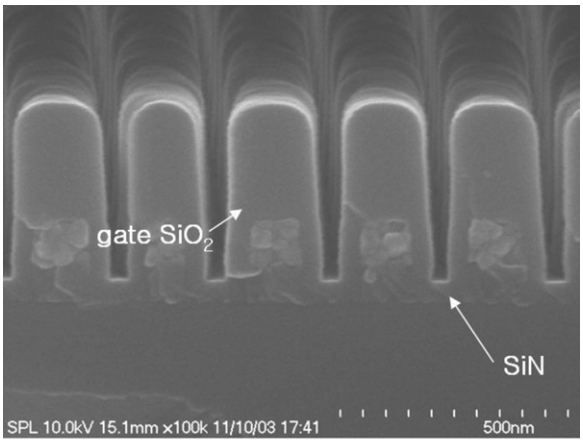

(a)

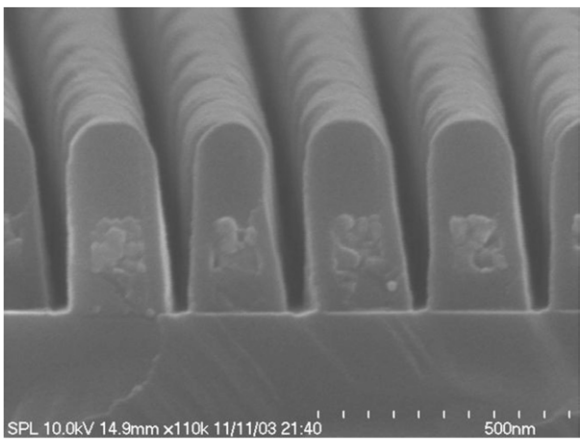

(b)

Figure 8. SEM etch profile after the Si_3N_4 spacer etching using a SF_6 neutral beam. (*a*) Before spacer etching and (*b*) after spacer etching. The figure is reprinted from [36].

4. Various applications of neutral beam etching

The neutral beam uses only reactive neutral particles. Therefore, the neutral beam might be applied to any material processing that has damage problems related to charging during the plasma processing if a reactive neutral beam can be applied to material processing. As a possible application, the neutral beam has been applied to the following processes: anisotropic etching of deep submicrometre features [27], photonic crystal (PC) formation on p-GaN to enhance the extraction efficiency of the GaN-based light emitting diode (LED) [37], surface treatment of screen printed carbon nanotubes (CNTs) for field emission displays (FED) [38], irradiation of a neutral beam for Ohmic contact formation to n-type GaN [39].

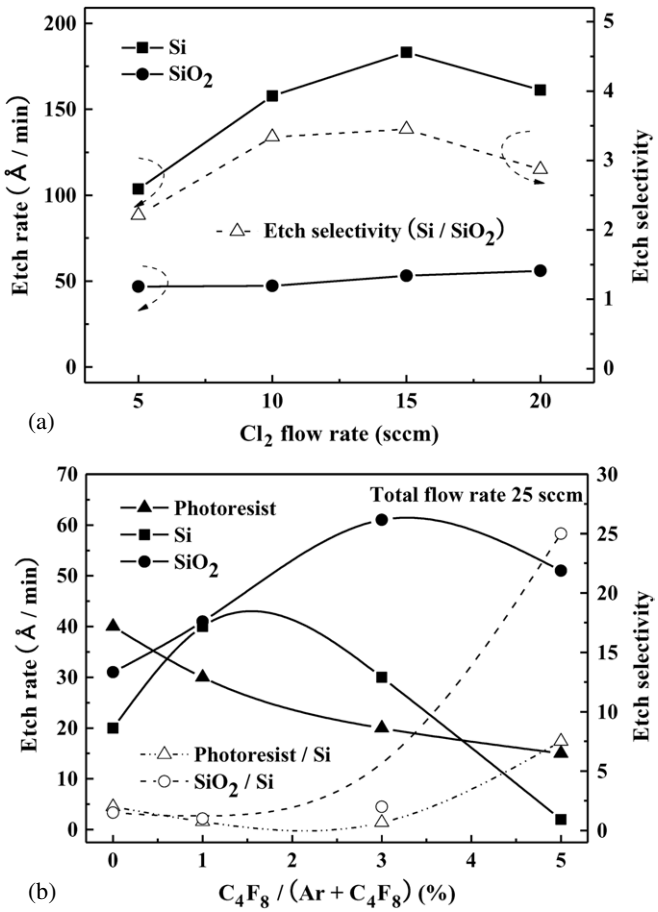

Figure 9. Etch rates of silicon and SiO_2 for (*a*) Cl_2 neutral beam and for (*b*) C_4F_8/Ar neutral beam (300 W of rf power, 400 V of acceleration voltage and -400 V of extraction voltage. Cl_2 flow rate was varied from 5 to 20 sccm while total C_4F_8/Ar flow rate was maintained at 25 sccm.)

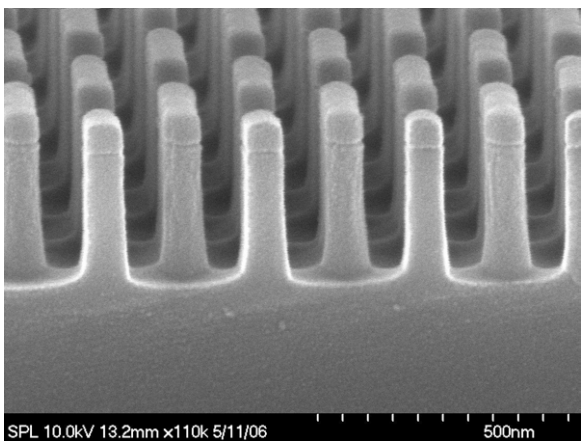

Figure 10. SEM micrograph of the Si etch profile obtained by using a Cl_2 neutral beam using the condition shown in figure 9.

4.1. Anisotropic etching of deep submicrometre features

Silicon-based features with a 50 nm width were etched using a neutral beam. Figure 9 shows the etch rates of silicon and SiO_2 for (*a*) Cl_2 neutral beam and for (*b*) C_4F_8/Ar neutral beam. Figure 10 shows the silicon etch profile. Etching was carried out at an rf power of 300 W, an acceleration voltage of 400 V and an extraction voltage of −400 V. The Cl_2 flow rate was varied from 5 to 20 sccm while the total C_4F_8/Ar flow rate was maintained at 25 sccm. Previously, the SF_6-based neutral beam was used to etch the silicon features. However, it was difficult to etch silicon anisotropically and selectively due to the excessive fluorine radicals existing during the etching by the SF_6 neutral beam [40]. Therefore, silicon-based features with a 50 nm width patterned using a silicon oxide-based hardmask were etched using a Cl_2-based neutral beam to increase the etch selectivity and etch anisotropically. As shown in figure 9(*a*), an increase in the Cl_2 flow rate to 15 sccm increased the etch selectivity of SiO_2/Si to approximately 3.5. Therefore, anisotropic silicon etching with 50 nm features could be achieved using this etch condition, as shown in figure 10.

A mixture of C_4F_8/Ar was used for selective SiO_2 etching. As shown in figure 9(*b*), the etch selectivity of SiO_2/Si increased with increasing C_4F_8 percentage in the gas mixture. An etch selectivity of SiO_2 to Si > 25 could be obtained when the C_4F_8 percentage was > 5%. It is believed that the selective nano-scale etching of Si and SiO_2 investigated using the above neutral beam can be applied to the gate and gate dielectric etching of future MOS devices, which are quite sensitive to the charging damage during gate etching.

4.2. Effect of neutral beam etching of p-GaN on the GaN device characteristics

Recently, various methods have been investigated to increase the emission efficiency of GaN-based LEDs for applications to flat panel displays, printers, traffic signals, the backlight for cell phones, exterior automotive lightening, etc. Among the various methods, the formation of surface roughness is the easiest way of improving the device efficiency. However, wet etching of GaN is difficult and does not provide a reliable and reproducible surface roughness. Using plasma etching instead of wet etching, more controlled surface roughness could be obtained on the GaN device. However, the p-GaN layer located on the top of a conventional GaN device is quite easily damaged by the energetic and charged species in the plasma [41, 42]. Degradation of the device properties caused by damage to the p-GaN layer and a multi-quantum well by plasma etching has been reported, even during the formation of PC [43, 44]. Therefore, a PC-like surface roughness was formed on the top p-GaN surface of a conventional GaN-based LED device using CF_4-based neutral beam etching, and its effects on the electrical and optical characteristics were examined.

Figure 11 shows the photoluminescence (PL) data of (*a*) undoped GaN, (*b*) p-type GaN (hole density of 2×10^{17} cm^{-3} by Mg doping) and (*c*) n-type GaN (electron density of 7×10^{17} cm^{-3} by silicon doping) measured after etching using ICP and a neutral beam with CF_4 [37]. The neutral beam source was a two-grid type. Rf power of 400 W, an acceleration voltage of 400 V and 15 sccm CF_4(25 Å min^{-1}) were used as the etch condition. The etch condition for ICP etching was an rf power of 400 W, a bias voltage of −400 V and 15 sccm CF_4 (1500 Å min^{-1}, working pressure: 0.7 mTorr). The etch depth was maintained at 750 Å for both etch conditions. So etching

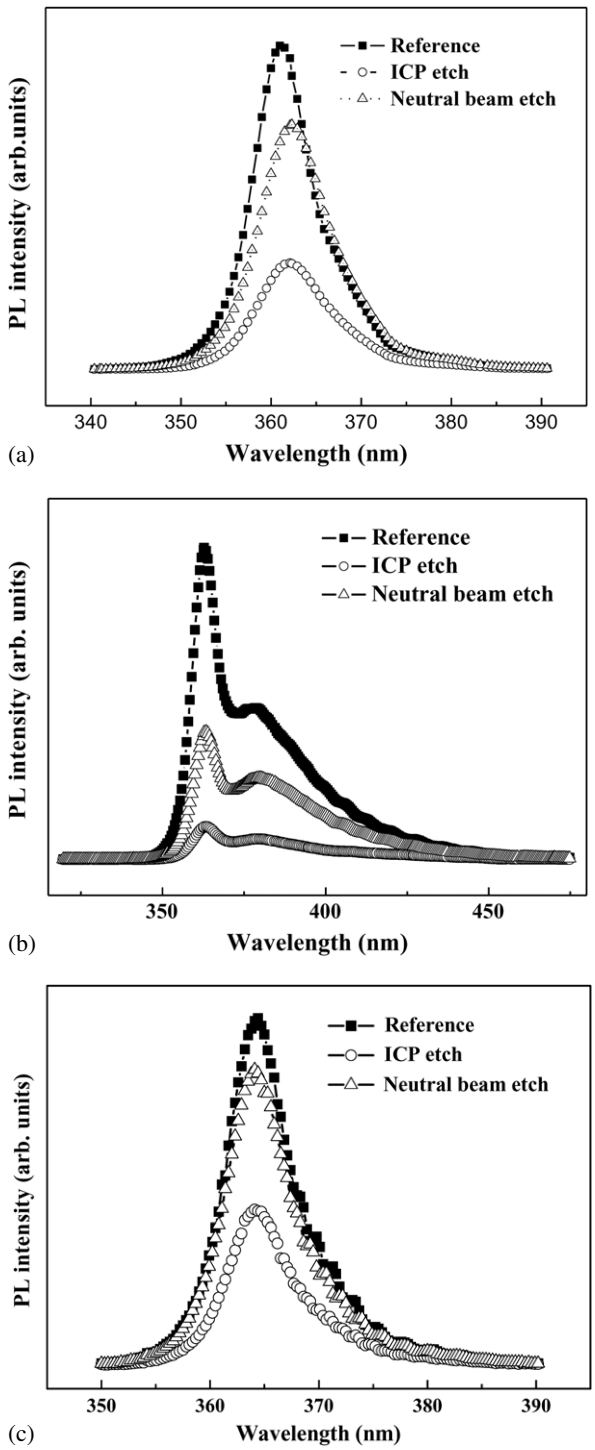

Figure 11. PL data of (*a*) undoped GaN, (*b*) p-type GaN and (*c*) n-type GaN after etching by the ICP (or ion beam) and the neutral beam using CF_4. The PL data of GaN without etching were included as references from [37].

time of ICP etching and neutral beam etching was, respectively, 30 s and 30 min. The PL data of the GaN obtained without etching were included as references. The PL was measured using a He–Cd laser (325 nm) at room temperature. As shown in figures 11(*a*) and (*b*), the PL intensities of the undoped and p-type GaN etched by the neutral beam decreased to less than those etched by ICP. In the case of n-GaN etched with the ion

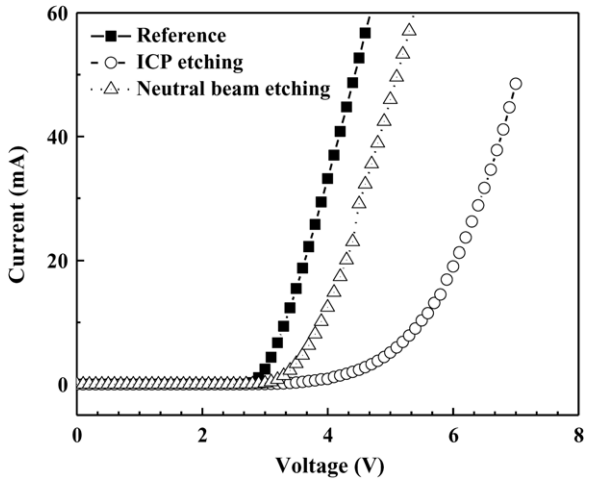

Figure 12. *I*–*V* characteristics of lateral GaN-based LED devices with the p-GaN etched by ICP and the neutral beam using the condition shown in figure 11. The figure is reprinted from [37].

beam in addition to the neutral beam, which was configured by removing the reflector from the neutral beam source under the same conditions, as shown in figure 11(*c*), the PL intensity of the n-GaN etched by the ion beam showed a more significant decrease compared with that etched by the neutral beam. Among the various GaN materials, the decrease in the PL intensity was most significant for p-GaN possibly indicating that p-GaN is the most significantly damaged among the GaN materials investigated. In addition, the damage by the ICP and ion beam was more significant than that by the neutral beam. Defect formation and implantation as interstitial impurities in GaN by energetic fluorine-based particle bombardment during etching can decrease the PL intensity, and defect formation and implantation can occur during all etching methods due to the similar particle bombardment energy of approximately 400 eV to the GaN surface during etching. However, there was less damage with neutral beam etching than with ICP etching or ion beam etching, which highlights the effect of charging during etching, which is possibly related to charge-induced defect formation.

Figure 12 shows the current–voltage (*I*–*V*) characteristics of the GaN-based LED devices fabricated after the formation of PC-like features on the p-GaN surface using the neutral beam and ICP. The etching conditions are the same as those shown in figure 11. As a reference, the *I*–*V* characteristic of the GaN-based LED fabricated without the formation of PC-like features are also included. As shown in figure 12, after the formation of a PC-like lens structure on p-GaN, the electrical characteristics were degraded for GaN-based LEDs treated with both ICP and the neutral beam [37]. However, the electrical characteristic of the ICP treated LED showed significant degradation, while that of the neutral beam treated LED was close to that of the reference. Degradation of the electrical characteristics after the formation of a PC-like lens structure is believed to be related to the damage formed on the p-GaN during etching.

The light emission characteristics of the above devices were compared using optical emission spectroscopy (OES). The results are shown in figure 13 for the optical emission

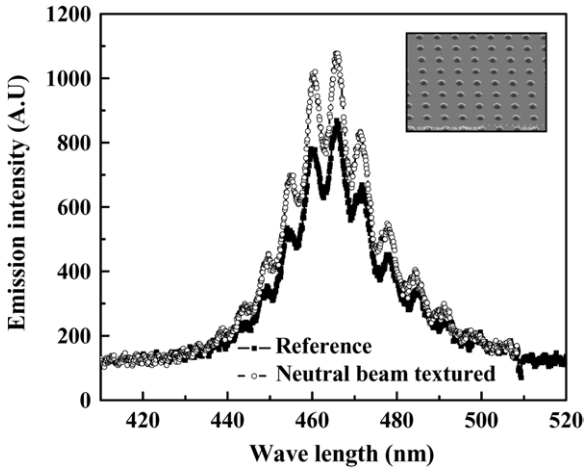

Figure 13. Light emission characteristics observed by OES. A 20 mA device current was employed for the optical emission spectra of the reference and neutral beam etched GaN LED devices. The figure is reprinted from [37].

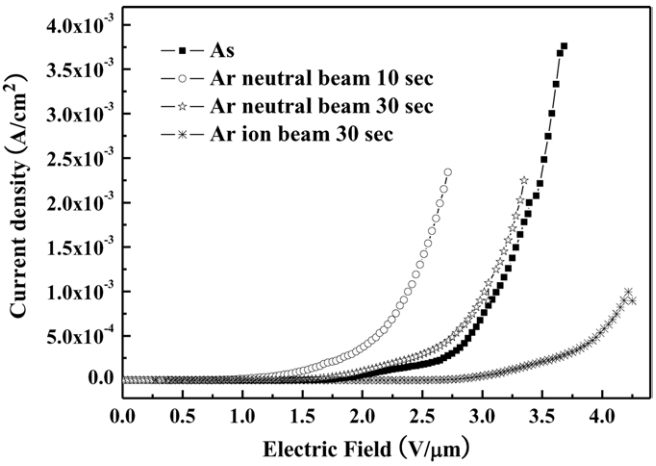

Figure 14. *I*–*V* characteristics of the screen printed CNTs treated by an Ar neutral beam (10 and 30 s) and an Ar ion beam (30 s) after adhesive tape activation. The neutral/ion beam treatment conditions were rf power of 200 W, an acceleration voltage of 100 V, an extraction voltage of −200 V and Ar gas. The figure is reprinted from [38].

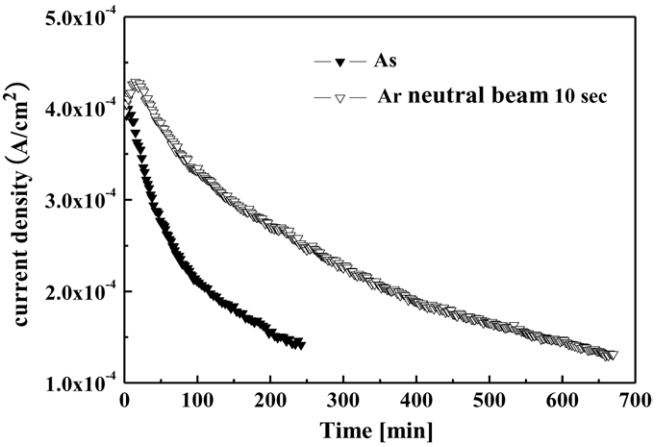

Figure 15. Long-term emission stability of the CNT emitter before and after the Ar neutral beam treatment for 10 s under the conditions shown in figure 14. The figure is reprinted from [38].

spectra of the reference and neutral beam treated devices at a device current of 20 mA. No light emission could be observed for the LED treated with ICP, indicating significant damage on the surface of p-GaN. However, as shown in the figure, the LED treated with the neutral beam showed an increase in emission intensity of approximately 20% compared with the reference due to the formation of a PC-like structure on the surface. The improved performance of the neutral beam etched GaN-based LED device compared with that etched by ICP is believed to be related to the lack of charge-induced defect formation on the p-GaN surface during the formation of PC-like features.

4.3. FED CNT paste treatment

Recently, CNT have been investigated for applications to field emission tips in FED on account of the excellent material and electrical properties of CNT [45–48]. One of the most conventional methods for applying CNTs as field emission tips is screen printing [49–51]. The CNTs are screen printed on a glass substrate. The CNT paste is then partially removed using adhesive tape peeling or by soft rubber rolling after baking the screen printed CNTs to expose and vertically align the CNTs. However, this method tends to leave a residue on the CNT surface [51–59]. The remaining residue can be removed by a plasma treatment after adhesive tape activation or soft rubber rolling. However, during the plasma treatment process, the long CNT emitters are bombarded intensively and cut by the positive ions due to the high electric field at the long CNT tip, resulting in a short length and damaged CNTs. Therefore, instead of a plasma treatment, the screen printed CNTs have been treated with an Ar neutral beam and an Ar ion beam after adhesive tape activation and the effects on the electrical properties of CNT emitters were investigated. The results are shown in figure 14 [38]. The neutral/ion beam treatment conditions were an rf power of 200 W, an acceleration voltage of 100 V, an extraction voltage of −200 V and Ar gas. As shown in figure 14, the turn-on field decreased from 1.65 to 0.60 V μm^{-1} after a 10 s treatment with the Ar neutral beam, and a decrease in turn-on field was observed up to a treatment time of 30 s. It is believed that the decrease in the turn-on field after the Ar neutral beam treatment is due to an increase in the number of activated CNT emitters by removing the residue without damaging the long exposed CNTs during the neutral beam treatment. Indeed, due to the energy of the neutral beam, the CNT surface could be also damaged by the neutral beam bombardment. Therefore, as shown in figure 14, the electrical properties of the Ar neutral beam treated CNTs showed slight degradation with increasing treatment time to 30 s. However, as shown in the figure, at the same treatment time of 30 s, the turn-on field of the CNT field emitter treated with the ion beam was higher than that treated with the neutral beam. Therefore, less damage was observed on the neutral beam treated CNT field emitter.

The long-term emission current stability of the neutral beam treated CNT field emitters was measured at a constant voltage of 1200 V before and after the neutral beam treatment for 10 s under similar conditions shown in figure 14. Figure 15

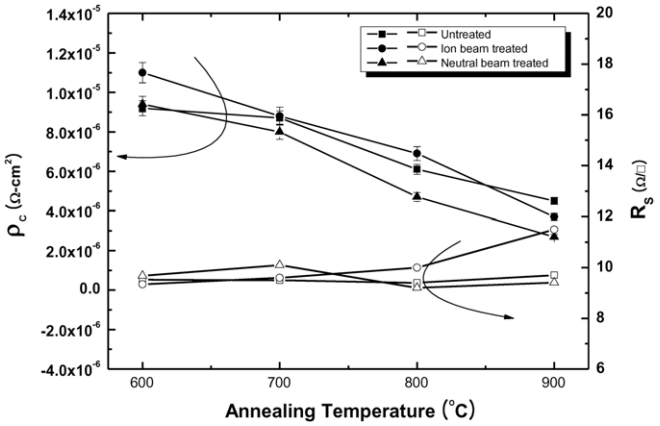

Figure 16. Specific contact resistivity and sheet resistance of n-GaN contact with Ti/Al/Au as a function of the annealing temperature (N_2 RTA for 30 s) after treating the n-GaN with a neutral beam and an ion beam before Ti/Al/Au metallization. The neutral/ion beam treatment condition was rf power of 300 W, an acceleration voltage of 400 V and 5 sccm of SF_6. The beam treatment time was 120 s. The figure is reprinted from [39].

shows the change in field emission current as a function of the operating time. As shown in the figure, significant degradation of the emission current density was observed after 240 min of operation on the untreated sample [38]. However, the CNT emitters treated with the Ar neutral beam for 10 s showed more stable emission properties than the untreated sample without any significant degradation or arcing during operation. Therefore, after the neural beam treatment, both the emission properties of the CNT emitter and the emission stability had improved.

4.4. Effect of fluorine neutral beam irradiation on Ohmic contact to n-GaN

Obtaining excellent Ohmic contact to GaN-based materials is one of the crucial steps in the fabrication of high-performance LEDs and laser diodes (LDs). There has been considerable effort on the formation of the low resistance Ohmic contact to n-type GaN-based materials using different metal schemes, such as Ti/Al- and V/Al-based metallization [60–64]. In conjunction with the above efforts, surface treatment techniques, such as wet treatment and plasma treatment, have also been proposed as an additional route to realize a good Ohmic contact [65, 66]. However, in the case of plasma treatments, the Ohmic contact properties can be degraded if the GaN surface is damaged by ion bombardment during treatment. Ping *et al* [67, 68] examined the effects of RIE-induced damage on the Schottky and Ohmic characteristics of n-GaN contacts.

The n-GaN surface was treated with fluorine ions and neutral beams, and their effects on the n-GaN Ohmic contact properties were investigated. Ohmic contacts were fabricated on n-type GaN surfaces treated by a fluorine neutral beam and a fluorine ion beam followed by evaporating the Ti/Al/Au contact metals sequentially, and their electrical characteristics were investigated. The neutral/ion beam treatment condition was an rf power of 300 W, an acceleration voltage of 400 V and 5 sccm of SF_6. The results are shown in figure 16. As shown in figure 16, the GaN Ohmic contact showed a lower contact resistivity after the beam treatments, and the GaN contact treated with the fluorine neutral beam showed the lowest contact resistivity of approximately $2.7 \times 10^{-6}\,\Omega\,\mathrm{cm}^2$ after annealing at 900 °C for 30 s using rapid thermal annealing (RTA) in N_2 [39]. Table 2 shows the composition of the n-GaN surface of the reference (as is), neutral beam treated, and ion beam treated samples with the condition shown in figure 16, as measured by x-ray photoelectron spectroscopy (XPS). As shown in the table, the GaN surface treated with both the fluorine neutral beam and the fluorine ion beam removed nitrogen preferentially from the surface [39]. Therefore, the contact resistivity was decreased by increasing the donor concentration near the surface. The decrease in contact resistivity by the beam treatment can be limited by the formation of surface defects and GaF_x compounds during the fluorine beam treatment. The GaF_x remaining on the GaN surface is an insulating material [65]. Figure 17 shows the narrow scan XPS data of Ga on the GaN surface treated with the fluorine neutral beam and the fluorine ion beam shown in figurre 16 [39]. As shown in the figure, less GaF_x was formed on the GaN surface treated with the neutral beam, which is possibly due to the lack of charge-induced defect formation and the lower reactivity of fluorine neutral compared with fluorine ion. Therefore, a lower contact resistivity could be obtained for GaN treated with the fluorine neutral beam compared with that treated with fluorine ion beam.

5. Summary and concluding remarks

This paper reviewed the characteristics of the neutral beam formed by low angle forward reflection and some of the application results obtained with the neutral beam.

The neutral beam fabricated by low angle forward reflection has a high neutralization efficiency higher than 99% even though its energy distribution and the degree of scattering need to be more investigated. Moreover, as one of the ion–electron surface neutralization methods, a large scale and uniform neutral beam can be generated in addition to the easy control of the energy and direction of the neutral beam. This neutral beam can be applied to the devices and materials that are sensitive to charge and UV radiation related damage during plasma processing such as plasma etching and plasma surface modification. For example, the etching of photoresist patterned polysilicon with different aspect ratios by the SF_6 neutral beam showed a negligible ARDE effect, which originated from charging during plasma processing. The application of a neutral beam to the etching of p-GaN and n-GaN showed less damage compared with the etching using an ICP possibly due to the lack of charge-induced damage formation during processing. When the neutral beam was applied to the screen printed CNT paste, there was a decrease in the turn-on field of the CNT field emitter due to the effective removal of surface residue remaining on the CNT surface without significant damage to the CNT field emission tip due to the lack of electric field enhanced bombardment of the protruding CNT tip.

Table 2. The composition of the n-GaN surface of the reference (as is), neutral beam treated, and ion beam treated samples under the conditions shown in figure 16, as measured by XPS. The table is reprinted from [39].

		Ion beam treated		Neutral beam treated	
	Untreated	Without BOE	With BOE	Without BOE	With BOE
Ga	45	25.8	52.9	27.3	53.4
N	45	24.9	37.8	24.4	37.9
F	0	25.3	0.95	14.4	0.4
O	10	24	8.35	33.8	8.3
GA/N	1	1.04	1.4	1.12	1.41

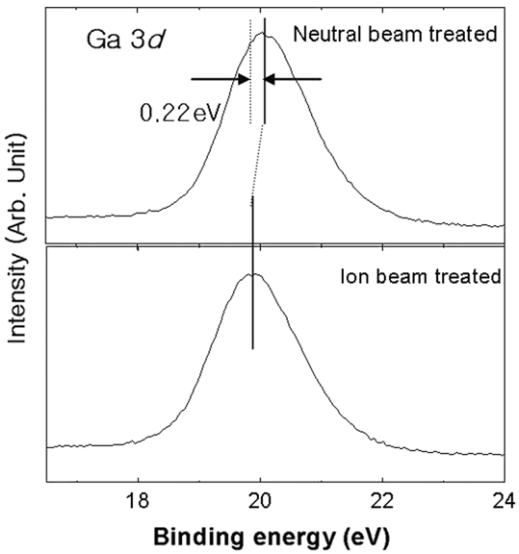

Figure 17. Narrow scan XPS data of Ga on the GaN surface treated by the fluorine neutral beam and fluorine ion beam reported in figure 16. The figure is reprinted from [39].

The most important application of the neutral beam is believed to be the gate/gate dielectric etching of sub nano-scale MOS devices. The current complementary MOS device structure may not necessarily require a neutral beam possibly due to the high thermal budget, which can remove electrical damage caused during the subsequent device thermal processing. However, as shown by the lack of a change in the breakdown voltage and the lack of threshold voltage shift in the MOS device after the neutral beam treatment, it is believed that when the critical dimension of the device is decreased to the sub-nano scale <50 nm, the allowed thermal budget will not be enough to remove all the charge-related damage caused by plasma processing. Therefore, a neutral beam may be required for the next generation device processing. In addition to the etching and surface modification, it is believed that the neutral beam can have many other applications in the near future, such as deposition and charge implantation, without charge-related damage.

Acknowledgment

This work was supported by the National Program for Tera-Level Nanodevices of the Korea Ministry of Science and Technology as a 21st Century Frontier Program.

References

[1] Yunogami T, Yokogawa K and Mizutani T 1995 Development of neutral-beam-assisted etcher *J. Vac. Sci. Technol.* A **13** 952–8
[2] Goeckner M J, Bennett T K, Park J Y, Wang Z and Cohen S A 1997 Reduction of residual charge in surface-neutralization-based neutral beams *Int. Symp. on Plasma Process-Induced Damage (AVS, Monterey, CA)*
[3] Yamamoto J, Kawasaki T, Sakaue H, Shingubara S and Horiike Y 1993 Digital etching study and Fabrication of fine Si lines and dots *Thin Solid Films* **225** 124–9
[4] Yokogawa K, Yunogami T and Mizutani T 1996 Neutral-beam-assisted etching system for low-damage SiO_2 etching of 8-inch wafers *Japan. J. Appl. Phys.* **35** 1902
[5] Leone S R 1995 Kinetic-energy-enhanced neutral etching *J. Appl. Phys.* **34** 2073–82
[6] Szabo A and Engel T 1994 Etching of Si surfaces with hot chlorine beams: translational and vibrational excitation of the incident chlorine particles *J. Vac. Sci. Technol.* A **12** 648–57
[7] Agnello P D 2002 Process requirements for continued scaling of CMOS-the need and prospects for atomic-level maniqulation *IBM J. Res. Dev.* **46** 317–38
[8] Giapis K P, Moore T A and Minton T K 1995 Hyperthermal neutral beam etching *J. Vac. Sci. Technol.* A **13** 959–65
[9] yamamoto J, Kawasaki T, Sakaue H, Shingubara S and Horiike Y 1993 *Thin Solid Films* **225** 124
[10] Suzuki K, Hiraoka S and Nishimatsu S 1988 Anisotropic etching of polycrystalline silicon with hot Cl_2 molecular beam *J. Appl. Phys.* **64** 3697–705
[11] Ono T, Kashima H, Hiraoka S and Suzuki K 1991 Anisotropic etching of gaas using a hot Cl_2 molecular beam *J. Vac. Sci. Technol.* B **9** 2798–801
[12] Geis M W, Efremow N N, Pang S W and Anderson A C 1987 Hot jet etching of Pb, GaAs, and Si *J. Vac. Sci. Technol.* B **5** 363–5
[13] Teraoka Y and Nishiyama I 1993 Anisotropic Si(1 0 0) etching induced by high translational energy Cl_2 molecular beams *Appl. Phys. Lett.* **63** 3355–7
[14] Hwang G S, Anderson C M, Gordon M J, Moore T A, Minton T A and Giapis K P 1996 Gas-surface dynamics and profile evolution during etching of silicon *Phys. Rev. Lett.* **77** 3049–52
[15] Yunogami T, Yokogawa K and Mizutani T 1995 *J. Vac. Sci. Technol.* A **13** 952
[16] Yokogawa K, Yunogami T and Mizutani T 1996 *Japan. J. Appl. Phys.* **35** 1901
[17] Yokogawa K, Yajima Y, Misutani T, Nishimatsu S and Ninomiya K 1991 *Japan. J. Appl. Phys.* **30** 3199
[18] Shimokawa F, Tanaka H, Uenishi Y and Sawada R 1989 Reactive-fast-atom beam etching of GaAs using Cl_2 gas *J. Appl. Phys.* **66** 2613–8

[19] Mizutani T and Nishimatsu S 1988 Sputtering yield and radiation damage by neutral beam bombardment *J. Vac. Sci. Technol.* A **6** 1417–20
[20] Tsuchizawa T, Jin Y and Matsuo S 1994 Generation of electron cyclotron resonance neutral stream and its application to Si etching *Japan. J. Appl. Phys. (Part 1)* **33** 2200–6
[21] Groeckner M J, Bennett T K and Cohen S A 1997 A Source of hyperthermal neutrals for materials processing *Appl. Phys. Lett.* **71** 980–2
[22] Panda S and Economou D J 2001 Anisotropic etching of polymer films by high energy (∼100 s of eV) oxygen atom neutral beams *J. Vac. Sci. Technol.* A **19** 398–404
[23] Samukawa S, Sakamoto K and Ichiki K 2002 Generating high-efficiency neutral beams by using negative ions in an inductively coupled plasma source *J. Vac. Sci. Technol.* **20** 1566
[24] Ranjan A, Donnelly V M and Economou D J 2006 Energy distribution and flux of fast neutrals and residual ions extracted from a neutral beam source *J. Vac. Sci. Technol.* A **20** 1839–46
[25] Lee D H, Bae J W, Park S D and Yeom G Y 2001 Development of a low angle forward reflected neutral oxygen beam for materials processing *Thin Solid Films* **398–399** 647–51
[26] Thumm U, Ducree J, Kurpick P and Wille U 1999 Charge transfer and electron emission in ion surface interactions *Nucl. Instrum. Methods Phys. Res.* B **157** 11–20
[27] Park B J, Min K S, Park S D, Bae J W, Vozniy O and Yeom G Y 2007 Formation of high flux parallel neutral beam using a three grid system of ion beam during low angle forward reflection of ions *Solid State Phenomena* **124–126** 275–8
[28] Chung M J, Lee D H and Yeom G Y 2002 Study on the low-angle forward-reflected neutral beam etching system for SiO2 etching *Thin Solid Films* **420–421** 579–83
[29] Lee D H, Chung M J, Park S D and Yeom G Y 2002 Damage during SiO_2 etching by low angle forward reflected neutral beam *Japan. J. Appl. Phys.* **41** 1412–5
[30] Kawamoto Y 1985 MOS gate insulator breakdown caused by exposure to plasma *Proc. 7th Dry Process Symp. (Tokyo)* (IEE) pp 132–7
[31] Lukaszek W, Quek E and Dixon W 1992 CHARM2: Towards an industry-standard wafer surface-charge monitor *IEEE/SEMI Advanced Semiconductor Manufacturing Conf. (Cambridge, MA)* pp 148–52
[32] Lukaszek W, Shields J and Birrell A 1997 Quantifying via charging currents *2nd Int. Symp. on Plasma Process-Induced Damage (Monterey, CA)*
[33] Gottscho R A, Jurgensen C W and Vitkavage D J 1992 Microscopic uniformity in plasma etching *J. Vac. Sci. Technol.* B **10** 2133
[34] Matsui J, Nakano N, Petrovic Z L and Makabe T 2001 The effect of topographical local charging on the etching of deep-submicron structures in SiO_2 as a function of aspect ratio *Appl. Phys. Lett.* **78** 883
[35] Hwang G S and Giapis K P 1999 Charging damage during residual metal overetching *Appl. Phys. Lett.* **74** 932–4
[36] Lee D H, Park B J and Yeom G Y 2005 Removal of aspect-ratio-dependent etching by low-angle forward reflected neutral-beam etching *J. Korean Phys. Soc.* **46** 867–71
[37] Park B J, Min K S, Lee H C, Bae J W, Kim D W and Yeom G Y 2007 Effect of neutral beam etching of p-GaN on the GaN device characteristics *J. Vac. Sci. Technol.* B **25** 295–8
[38] Kyung S J, Park J B, Park B J, Min K S, Lee J H and Yeom G Y 2007 The effect of Ar neutral beam treatment of screen-printed carbon nanotubes for enhanced field emission *J. Appl. Phys.* **101** 083305-1-5
[39] Lee H C, Bae J W, Park B J, Jang J H and Yeom G Y 2007 Effect of fluorine ion/neutral-beam irradiation on ohmic contact formation to n-type GaN *Electrochem. Solid-State Lett.* **10** H161-4
[40] Lee D H, Park B J, Min K S and Yeom G Y 2006 CF4-based neutral-beam etch characteristics of Si and SiO2 using a low angle forward reflected neutral-beam etching system *J. Korean Phys. Soc.* **49** 2307–10
[41] Cao X A, Pearton S J, Zhang A P, Dang G T, Ren F, Shul R J, Zhang L, Hickman R and Van Hove J M 1999 Electrical effects of plasma damage in p-GaN *Appl. Phys. Lett.* **75** 2569–71
[42] Lee J M, Lee K S and Park S J 2004 Removal of dry etch damage in p-type GaN by wet etching of sacrificial oxide layer *J. Vac. Sci. Technol.* B **22** 479–82
[43] Kim D W, Sung Y J, Park J W and Yeom G Y 2001 A study of transparent indium tin oxide (ITO) contact to p-GaN *Thin Solid Films* **398-9** 87–92
[44] Huh C, Lee K S, Kang E J and Park S J 2003 Improved light-output and electrical performance of InGaN-based light-emitting diode by microroughening of the p-GaN surface *J. Appl. Phys.* **93** 9383-5
[45] Ajayan P M, Stephan P, Coliex C and Trauth D 1994 Aligned carbon nanotube arrays formed by cutting a polymer resin–Nanotube Composite *Science* **265** 1212–4
[46] Liu C, Fan Y Y, Liu M, Cong H T, Cheng H M and Dressel M S 1999 Hydrogen storage in single-walled carbon nanotubes at room temperature *Science* **286** 1127–9
[47] De Heer W A, Chatelain A and Ugarte D A 1995 A carbon nanotube field-emission electron source *Science* **270** 1179–80
[48] Lee Y H, Jang Y T, Kim D H, Ahn J H and Ju B 2001 Realization of gated field emitters for electrophotonic applications using carbon nanotube line emitters directly grown into submicrometer holes *Adv. Mater. (Weinheim, Germany)* **13** 479–82
[49] Shi Y S, Zhu C C, Qikun W and Xin L 2003 Large area screen-printing cathode of CNT for FED *Diamond Relat. Mater.* **12** 1449–52
[50] Lee S R, Im W B, Kang J H and Jeom D Y 2005 Low temperature burnable carbon nanotube paste component for carbon nanotube field emitter backlight unit *J. Vac. Sci. Technol.* B **23** 745–8
[51] Yukui L, Changchun Z and Xinghui L 2002 Field emission display with carbon nanotubes cathode: prepared by a screen-printing process *Diamond Relat. Mater.* **11** 1845–7
[52] Vink T J, Gillies M, Kriege J C and Van de larr H W J J 2003 Enhanced field emission from printed carbon nanotubes by mechanical surface modification *Appl. Phys. Lett.* **83** 3552–4
[53] Liu Y, Liu L, Liu P, Sheng L and Fan S 2004 Plasma etching carbon nanotube arrays and the field emission properties *Diamond Relat. Mater.* **13** 1609–13
[54] Kim J S, Ahn K S, Kim C O and Hong J P 2003 Ultraviolet laser treatment of multiwall carbon nanotubes grown at low temperature *Appl. Phys. Lett.* **82** 1607–9
[55] Kim Y C, Sohn K H, Cho Y M and Yoo E H 2004 Vertical alignment of printed carbon nanotubes by multiple field emission cycles *Appl. Phys. Lett.* **84** 5350–2
[56] Kim D H, Kim C D and Lee H R 2004 Effects of the ion irradiation of screen-printed carbon nanotubes for use in field emission display applications *Carbon* **42** 1807–12
[57] Zhu Y W, Cheong F C, Yu T, Xu X J, Lin C T and Thong J T L 2005 Effects of CF plasma on the field emission properties of aligned multi-wall carbon nanotube films *Carbon* **43** 395–400

[58] Ahn K S, Kim J S, Kim C O and Hong J P 2003 Non-reactive rf treatment of multiwall carbon nanotube with inert argon plasma for enhanced field emission *Carbon* **41** 2481–5
[59] Kung S C and Hwang K C 2002 Oxygen and ozone oxidation-enhanced field emission of carbon nanotubes *Appl. Phys. Lett.* **80** 4819–21
[60] Qiao D, Yu L S, Jia L, Asbeck P M, Lau S S and Haynes T E 2002 Transport properties of the advancing interface ohmic contact to AlGaN/GaN heterostructures *Appl. Phys. Lett.* **80** 992–4
[61] Jeon C M, Jang H W, Choi K J, Bae S B, Lee J H and Lee J L 2002 Fabrication of AlGaN/GaN heterostructure field effect transistor using room-temperature ohmic contact *Solid-State Electron.* **46** 695–8
[62] Hilsenbeck J, Rjeger W, Nebauer E, John W, Trankle G, Wiirfl J, Ramakrishnan A and Obloh H 1999 AlGaN/GaN HFETs with new ohmic and Schottky contacts for thermal stability up to 400 °C *Phys. Status Solidi* a **176** 183–7
[63] Ruvimov S, Liliental-Weber Z, Washburn J, Qiao D, Lau S S and Chu P K 1998 Microstructure of Ti/Al ohmic contacts for n-AlGaN *Appl. Phys. Lett.* **73** 2582–4
[64] Schweitz K O, Wang P K, Mohney S E and Gotthold D 2003 V/Al/Pt/Au Ohmic contact to n-AlGaN/GaN heterostructures *Appl. Phys. Lett.* **80** 1954–6
[65] Lin M E, Fan Z F, Ma Z, Allen L H and Morkoc H 1994 Reactive ion etching of GaN using BCl_3 *Appl. Phys. Lett.* **64** 887–8
[66] Ping A T, Chen Q, Yang J W, Khan M A and Adesida I 1998 The effect of reactive ion etching-induced damage on the characteristics of ohmic contacts to n-type GaN *J. Electron. Mater.* **27** 261–5
[67] Ping A T, Schmitz A C, Chen Q, Yang J W, Khan M A and Adesida I 1997 Characterization of reactive ion etched-induced damage to n-GaN surfaces using Schottky diodes *J. Electron. Mater.* **26** 266–72
[68] Simpson W C, Durbin T D, Varekamp P R and Yarmoff J A 1995 The growth of GaF_3 films on GaAs(1 1 0) at elevated temperatures studied with soft x-ray photoelectron spectroscopy *Appl. Phys. Lett.* **77** 2751–8